Biochimica et Biophysica Acta 1812 (2011) 1452–1459

Contents lists available at ScienceDirect

Biochimica et Biophysica Acta

journal homepage: www.elsevier.com/locate/bbadis

Identification and functional characterization of KCNQ1 mutations around the exon 7–intron 7 junction affecting the splicing process

Keiko Tsuji–Wakisaka [a], Masaharu Akao [b], Takahiro M. Ishii [c], Takashi Ashihara [a], Takeru Makiyama [b], Seiko Ohno [b], Futoshi Toyoda [d], Kenichi Dochi [a], Hiroshi Matsuura [d], Minoru Horie [a,*]

[a] Department of Cardiovascular and Respiratory Medicine, Shiga University of Medical Science, Otsu, Japan
[b] Department of Cardiovascular Medicine, Kyoto University Graduate School of Medicine, Kyoto, Japan
[c] Department of Physiology, Kyoto University Graduate School of Medicine, Kyoto, Japan
[d] Department of Physiology, Shiga University of Medical Science, Otsu, Japan

ARTICLE INFO

Article history:
Received 17 March 2011
Received in revised form 28 June 2011
Accepted 18 July 2011
Available online 24 July 2011

Keywords:
Long QT syndrome
Ion channel
Splicing mutation

ABSTRACT

Background. KCNQ1 gene encodes the delayed rectifier K^+ channel in cardiac muscle, and its mutations cause long QT syndrome type 1 (LQT1). Especially exercise-related cardiac events predominate in LQT1. We previously reported that a KCNQ1 splicing mutation displays LQT1 phenotypes. *Methods and results*. We identified novel mutation at the third base of intron 7 (IVS7 +3A>G) in exercise-induced LQT1 patients. Minigene assay in COS7 cells and RT-PCR analysis of patients' lymphocytes demonstrated the presence of exon 7-deficient mRNA in IVS7 +3A>G, as well as c.1032G>A, but not in c.1022C>T. Real-time RT-PCR demonstrated that both IVS7 +3A>G and c.1032G>A carrier expressed significant amounts of exon-skipping mRNAs (18.8% and 44.8% of total KCNQ1 mRNA). Current recordings from *Xenopus* oocytes injected cRNA by simulating its ratios of exon skipping displayed a significant reduction in currents to 64.8 ± 4.5% for IVS7 + 3A>G and to 41.4 ± 9.5% for c.1032G>A carrier, respectively, compared to the condition without splicing error. Computer simulation incorporating these quantitative results revealed the pronounced QT prolongation under beta-adrenergic stimulation in IVS7 +3A>G carrier model. *Conclusion*. Here we report a novel splicing mutation IVS7 +3A>G, identified in a family with mild form LQT1 phenotypes, and examined functional outcome in comparison with three other variants around the exon 7–intron 7 junction. In addition to c.1032G>A mutation, IVS7 +3A>G generates exon-skipping mRNAs, and thereby causing LQT1 phenotype. The severity of clinical phenotypes appeared to differ between the two splicing-related mutations and to result from the amount of resultant mRNAs and their functional consequences.

1. Introduction

Long QT syndrome (LQTS) is characterized by prolongation of the cardiac action potential, syncopal attacks, torsades de pointes arrhythmias and sudden cardiac death [1–3]. The slow component of delayed rectifier K^+ current (I_{Ks}) in the heart modulates repolarization of cardiac action potential. The I_{Ks} channel is formed by the co-assembly of KCNQ1 α-subunits and KCNE1 β-subunits [4,5]. Mutations in the KCNQ1 cause the most frequent form of inherited LQT1 [6]. Exercise-related cardiac events dominate the clinical picture of LQT1 patients.

Pre-mRNA processing is an important aspect of gene expression and consists of the precise recognition of exons and removal of introns in such a way that the exons are joined to form mature mRNAs with intact translational reading frames [7,8]. Disruption of normal splicing as a result of genetic mutation can lead to the generation of abnormal proteins or the degradation of aberrant transcripts through nonsense-mediated decay, and thus to the pathogenesis of a variety of human diseases [9].

We previously reported three LQTS families, in whom a G to A change in the last base of KCNQ1 exon 7 (c.1032G>A) was identified [10]. The mutation alters the 5′ splice-site of intron 7, resulting in the production of exon-skipping transcripts, but not to alter the coded alanine (A344A) [11,12], since it involves the characteristic consensus sequence of the splicing donor site, A***G***/GUAAGU. The vicinity of junction around the KCNQ1 exon 7–intron 7 appeared to be a hot area for genetic variants that may potentially cause aberrant splicing, and we identified a novel mutation that changes an A to G at the third base of intron 7 (IVS7 +3A>G) in LQTS family with mild clinical phenotypes. In contrast, another neighboring KCNQ1 mutation, c.1022C>T (p. A341V) is known to produce severe clinical phenotypes [13].

To test the potential influence of these mutations that may affect the KCNQ1 splicing, we established a minigene assay system in which a respective mutant construct is transcribed in COS7 cells and examined the genetic and biophysical characterization of the novel IVS7 +3A>G

* Corresponding author at: Department of Cardiovascular Medicine, Shiga University of Medical Sciences, Japan. Tel.: +81 77 548 2213; fax: +81 77 543 5839.
E-mail address: horie@belle.shiga-med.ac.jp (M. Horie).

0925-4439/$ – see front matter © 2011 Elsevier B.V. All rights reserved.
doi:10.1016/j.bbadis.2011.07.011

mutation. For comparison, we also investigated two other mutations around the exon 7–intron 7 junction; c.1022C>T and c.1032G>A. We quantitatively analyzed the aberrant splicing and its functional consequences and then carried out a computer simulation to explore how this mutation could be associated with exercise-induced QT prolongation and tachyarrhythmias.

2. Materials and methods

2.1. Genomic DNA isolation and mutation analysis

Mutation analysis was carried out as previously described [10]. Genomic DNA was prepared from peripheral blood leukocytes. Sixteen exons of the KCNQ1 gene were amplified by PCR. Genetic screening was performed for KCNQ1 by denaturing high-performance liquid chromatography (DHPLC) using a WAVE System Model 3500 (Transgenomic: Omaha, NE). We optimized the running optimum temperature at 64.6 °C. Abnormal conformers were amplified by PCR and sequencing was performed on an ABI PRISM3130 DNA sequencer (Applied Biosystems: Foster City, CA). We also carried out a complete screening for other LQTS-causing genes; KCNH2, SCN5A, KCNE1, KCNE2, and KCNJ2.

2.2. Construction of splicing minigene and transfection

Exon 7 of the KCNQ1 gene (111 bps) and its flanking introns (507 bps at 5′ arm and 453 bps at 3′ arm) were amplified by PCR using genomic DNA from control and patients. PCR fragments were cloned into the pSPL3 exon trapping vector (Gibco BRL) digested with *EcoRV* within the multiple cloning site. The pSPL3 vector contains the HIV-1 tat exons and the intervening intron with *EcoRV* site. COS7, CHO and HL-1cells were transfected with 0.25 μg plasmid DNA using Lipofectamin transfection reagent (Invitrogen). Cells were harvested 48 h post-transfection.

2.3. RNA extraction and RT-PCR

Total cellular RNA was isolated with QIAamp RNA Blood Mini Kits (Qiagen). Subsequently, total RNA was reverse-transcribed by use of the SuperScriptIII FirstStrand Synthesis System (Invitrogen: Carlsbad, CA), and was used as a template for subsequent PCR reactions. We used the forward primer (5′-TCTGAGTCACCTGGACAACC-3′) and the reverse primer (5′-ATCTCAGTGGTATTTGTGAGC-3′), both of which anneal to the pSPL3 vector sequence.

Total RNA was extracted from leukocytes of fresh blood and was reverse-transcribed using the same methods described above. Using the cDNAs as templates, PCR amplification was performed with the exon 5-F forward primer (5′-GGGCATCCGCTTCCTGCAGA-3′) and the exon10-R reverse primer (5′-CCATTGTCTTTGTCCAGCTTGAAC-3′) to amplify KCNQ1 cDNA from exons 5 through 10.

Measurements of normal and mutant mRNA levels were performed by real-time RT-PCR by use of an ABI PRISM 7900HT Sequence Detection System (Applied Biosystems). The reaction mixture contained SYBR Green PCR Master Mix (Applied Biosystems), cDNA template, and PCR primers. In order to selectively amplify these splicing variants, PCR primers were designed so that they spanned the adjacent exons: exon 6.8-F: 5′-CTGTGGTGGGGGGTG-GGGATT-3′, exon 6.9-F: 5′-TGTGGTGGGGGGTG-ACCGCAT-3′, and exon 7.9-F: 5′-CTTTGCGCTCCCAGCG-ACCG-3′ (all the hyphens inside the primer sequence indicate the boundaries of exons). In all cases, the dissociation curves showed that there was no significant contribution of relatively short by-products to the measured fluorescence intensities.

All the samples were tested in duplicate. A standard curve for each primer pair was obtained using serial dilutions of a recombinant plasmid containing cDNA. The threshold cycle (Ct) was subsequently determined. Relative mRNA levels of splice mutants were calculated based on the Ct values and normalized by the GAPDH level of each sample. The amounts of mutant cDNA were expressed as a percentage of the total KCNQ1 mRNA, for which exons 9 through 10 were amplified with the exon 9-F forward primer (5′-CGCATGGAGGTGC-TATGCT-3′) and the exon 10-R reverse primer.

2.4. Oocyte isolation and electrophysiology

Xenopus laevis oocytes were prepared and current recordings were carried out as described previously [14]. Wild-type (WT) cRNA plus mutant-cRNA (total 10 ng) was injected into *Xenopus* oocytes. All the current recordings in the present study were performed in the presence of KCNE1 β-subunits (1 ng). An axoclamp-2B amplifier (Axon Instruments: Union City, CA) was used to record currents at 25 °C in oocytes 3–4 days after cRNA injection, using standard two-electrode voltage-clamp techniques. To decrease the interference from endogenous Cl^- current, we used a low-Cl^- bath solution (mM): NaOH 96, KOH 2, $CaCl_2$ 2, $MgCl_2$ 1, MeS 101, HEPES 5 (pH titrated to 7.6 with methanesulfonic acid). Currents were sampled at 10 kHz and filtered at 2 kHz. Voltage steps were applied with 3-second pulses in 10 mV increments from a holding potential of −80 mV to voltages from −70 to +30 mV, and then to −30 mV. Current amplitudes were measured at 1.8-second after the initiation of 3-second pulse applied to a +30 mV test potential, followed by the subtraction of background I_{Ks} current (22.9 nA).

2.5. Computer simulation

We conducted simulations of paced propagation in a one-dimensional (1D) bidomain myocardial model of 9.0-mm length with transverse conductivity, mimicking transmural section of left ventricular free wall. Membrane kinetics was represented by the Priebe–Beuckelmann model [15], which can simulate human ventricular action potentials.

To obtain the ventricular transmural gradient, we defined endocardial, mid-myocardial, and epicardial tissues of lengths (thicknesses) 0.6 mm, 6.0 mm, and 2.4 mm, respectively, and then we incorporated modifications of ion channel conductance (Table 1), based on the previous studies [16,17]. Pacing stimuli of 3-ms duration and strength twice-diastolic threshold were applied transmembranously to the endocardial end at a cycle length of 1000 ms. To get ECG similar to the left precordial ECG, a unipolar recording electrode was located 3 cm above the epicardial end of the tissue. Other model parameters, such as the tissue conductivities and the boundary conditions, can be found elsewhere [18,19].

To achieve the beta-adrenergic stimulation, we set the parameters as previously described [20–22]: (1) shifting the fast and slow inactivation curves of the sodium current (I_{Na}) –3.4 mV, (2) increasing the L-type calcium current (I_{CaL}) 3 times and slowing the time constant of inactivation 1.13 times, (3) increasing the half-point concentration for the calcium-dependent inactivation (f_{Ca}) from 0.7 to 0.9 μM, and setting its non-zero minimum value to 0.03, (4) increasing the slowly

Table 1
Model modification values for ventricular transmural gradient.

	Endo	M	Epi
G_{Ks}	208%	52%	280%
G_{K1}	82%	83%	100%
G_{NaCa}	72%	108%	100%
G_{to}	25%	87%	100%
G_j	100%	100%	76%

G_{Ks}, conductance of slowly activating component of delayed rectifier potassium channel; G_{K1}, conductance of inward rectifier potassium channel; G_{NaCa}, conductance of sodium–calcium exchanger; G_{to}, conductance of transient outward potassium channel; G_j; gap junctional conductance. All values are expressed in percentage compared to original values [15]. Endo; endocardial cell, M; midcardial cell, Epi; epicardial cell.

activating component of delayed rectifier potassium current (I_{Ks}) 2 times and shifting the activation curve −8 mV, and (5) increasing currents of the calcium pump in sarcoplasmic reticulum (I_{up}) and the sodium–potassium pump (I_{NaK}) 1.41 and 1.2 times, respectively.

The numerical approach, including methods for integration and solution of the linear system, has been described elsewhere [18]. The time and spatial discretization steps were 10 μs and 75 μm, respectively. The method for calculating ECG was also described previously [23]. QT interval was numerically defined as the time period from the onset of Q wave to the last peak of second derivative of T wave. The convergence of the simulation results was tested by repeating some simulations with half of the spatial and time discretization steps.

2.6. Statistical analysis

Quantitative data are presented as the mean ± SEM. Multiple comparisons among groups were carried out by one-way ANOVA with Bonferroni's least significant difference as the post-hoc test. A level of $P<0.05$ was accepted as statistically significant.

3. Results

3.1. Clinical phenotypes

Pedigree for the family with novel IVS7 + 3A>G mutation is shown in Fig. 1a. The proband, 34-year-old woman (II-1), was first diagnosed with LQTS at age 14, and has remained asymptomatic. The ECG recording at rest showed a marked QT prolongation ($QT_c = 558$ ms: Fig. 1b). Her mother (I-2) had no syncopal episodes, despite a remarkable QT prolongation at rest ($QT_c = 536$ ms: Fig. 1b, I-2). Her father (I-1) had normal QT_c interval ($QT_c = 367$ ms: Fig. 1b, I-1). None of her relatives have had a history of syncope or cardiac sudden death. Treadmill test of the proband revealed a pronounced exercise-induced QT prolongation ($QT_c = 503$ ms before exercise, 615 ms at stage 4: Fig. 1c).

Regarding the families with c.1032G>A mutation, there were 9 probands from 9 unrelated families. Eight of them (89%) were symptomatic, and seven (78%) developed cardiac events before age 15. Their episodes were triggered by exercise, especially swimming (five cases). Seven of 9 families (78%) had at least >2 symptomatic mutation carriers.

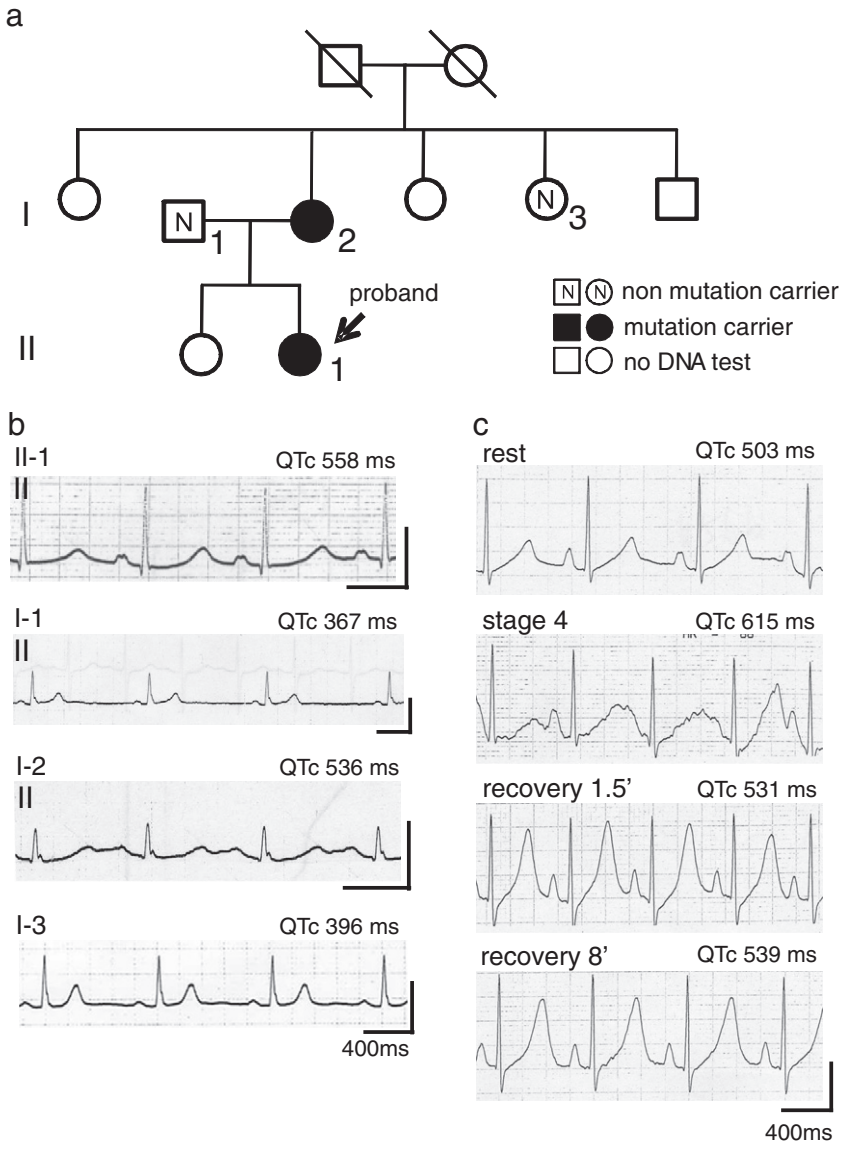

Fig. 1. Clinical and genetic characteristics of the family. (a) Pedigree. Circles represent females and squares represent males. The arrows indicate the proband. Members carrying the mutation are represented by solid symbols. (b) ECG recordings. ECG panels show ECG recordings at rest of various individuals. The QTc interval is indicated. (c) ECG recordings at treadmill exercise test.

Mean QT_c interval of 9 probands were 494 ± 90 ms. Although there is only one family with IVS7 +3A>G mutation, clinical features were apparently severer in families with c.1032G>A mutation.

3.2. Mutation analysis

DNA samples from 3 members of the family were subjected to a mutation screening of the KCNQ1 gene. An abnormal migration pattern was identified by DHPLC analysis (Fig. 2a; note the greater height of the left peak in II-1 and I-2 as indicated by the arrows) in KCNQ1 exon 7 of the 2 affected individuals. The control sample and the father (I-1) showed a normal pattern, as indicated by the comparable height of the left and right peaks (Fig. 2a). DNA sequencing identified a heterozygous adenine to guanine transition in KCNQ1 at nucleotide IVS7 + 3 (IVS7 +3A>G) (Fig. 2b right panel), which located in the 5′ splice-site of intron 7. Fig. 2b left panel shows a schematic structure of KCNQ1 channel subunit. The exon 7 spans from part of the P-loop to part of the S6 region (indicated by red color).

3.3. Screening of KCNQ1 splicing mutation using minigene assay

Minigene assay was performed in COS7 cells to assess the effect of the IVS7 +3A>G mutation on the splicing of KCNQ1 exon 7. Fig. 3a shows the construct of minigene harboring KCNQ1 exon 7 and its flanking introns inserted into the pSPL3 vector. We also tested 3 other neighboring mutations that may affect the splicing of exon 7 (c.1022C>T, c.1032G>A, IVS7 +28T>C). c.1032G>A was used as a positive control that we and others reported to cause skipping of exon 7 [10,12].

The control KCNQ1 minigene expression in COS7 cells resulted in a production of the single mRNA band that corresponds to KCNQ1 exon 7 joined to the vector exons (Fig. 3b). The mutant minigene containing c.1022C>T or IVS7 +28T>C also showed the same single mRNA, indicating these mutations do not cause aberrant splicing (Fig. 3b). However, the mutant minigene containing IVS7 + 3A>G, as well as the positive control c.1032G>A, generated 2 major mRNA bands that correspond to the normal transcript and a shorter transcript lacking KCNQ1 exon 7 respectively (Fig. 3b). The expression level of the shorter mRNA band appeared to be greater in c.1032G>A compared with IVS7 + 3A>G. No band was detected in the RNA sample without reverse-transcriptase. We confirmed similar results both in CHO and HL-1cells under the same experimental conditions (data not shown).

3.4. Identification of exon-skipping KCNQ1 mRNAs in patient's blood sample

To directly confirm the minigene assay results, total RNA samples extracted from the patients' lymphocytes were subjected to RT-PCR (Fig. 4a), using primers spanning exons 5 through 10. Samples from individuals having IVS7 +3A>G and c.1032G>A showed shorter bands as well as the normal-sized WT. The direct sequencing of these short-sized transcripts revealed the existence of three kinds of exon-skipping mRNAs as indicated to the right of panel 4a (Δ7-8:399 bp, Δ7: 495 bp, Δ8: 510 bp, WT: 606 bp). Nucleotide sequence of each of the exon-skipping mRNAs is also shown. Control, c.1022C>T and IVS7 +28T>C showed normal patterns; the predominant WT and a small portion of Δ8.

3.5. Quantification of exon-skipping KCNQ1 mRNAs using real-time RT-PCR

We carried out quantitative analysis of short-sized mutant mRNAs in affected patients carrying the IVS7 +3A>G or c.1032G>A mutation, using real-time RT-PCR. Normal individuals had minor fractions of splicing variants (WT: 93.0 ± 0.7%, Δ7: 0.0 ± 0.0%, Δ7-8: 0.1 ± 0.0%, Δ8: 6.9 ± 0.7%, of total KCNQ1 transcripts; n = 4) as shown in the left bar graph of Fig. 4b. In contrast to c.1032G>A carriers who displayed a distinct exon skipping (WT: 55.2 ± 0.9%, Δ7: 23.5 ± 1.7%, Δ7-8: 16.8 ± 0.9%, Δ8: 4.5 ± 0.7%; n = 3, right bar graph in panel 4b), IVS7 +3A>G carrier showed modest but significant amount of exon skipping (WT: 81.2%, Δ7: 9.7%, Δ7-8: 5.7%, Δ8: 3.4%; n = 1, middle bar graph).

3.6. Biophysical characteristics of exon-skipping KCNQ1 proteins

Previously, we performed biophysical characterization of mutant KCNQ1 proteins (Δ7, Δ7-8, and Δ8) in *X. laevis* oocytes injected with mutant cRNAs. We demonstrated the *Xenopus* oocytes injected with Δ7, Δ7-8, or Δ8 alone displayed no time-dependent currents, indicating these mutants were non-functional. Furthermore, each exon-skipping KCNQ1 protein had the mutant-specific level of dominant-negative effect on WT channels [10].

In order to simulate the electrophysiological properties of cardiac cells of the affected patients, we injected the cRNAs (total 10 ng) with the relative ratios of WT and mutant KCNQ1 inferred from the data obtained in the real-time RT-PCR experiment (Fig. 4b). Oocytes injected at cRNA ratios comparable to those evaluated in IVS7 +3A>G showed remarkable reduction in currents compared with those of normal individuals, but less pronounced than c.1032G>A carriers; 100 ± 14.5% (n = 6) for control, 64.8 ± 4.5% (n = 7) for IVS7 +3A>G carriers ($p<0.05$), 41.4 ± 9.5% (n = 6) for c.1032G>A carriers ($p<0.05$) (Fig. 5).

3.7. Computer simulation

Finally, we performed a computer simulation study employing the 1D myocardial model (Fig. 6a) to explore the cellular mechanisms by which these splicing mutations manifest QT prolongation under exercise and induce ventricular tachyarrhythmias.

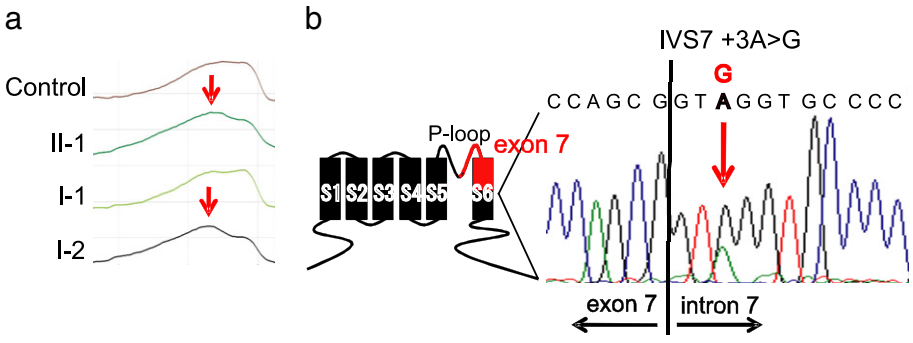

Fig. 2. Mutation analysis. (a) DHPLC revealed abnormal migration patterns in the affected individuals. (b) Left panel: scheme of the transmembrane topology of the cardiac KCNQ1 channel illustrating the location of exons 7 (red). Right panel: automated DNA sequencing electropherogram demonstrates IVS7 +3A>G mutation.

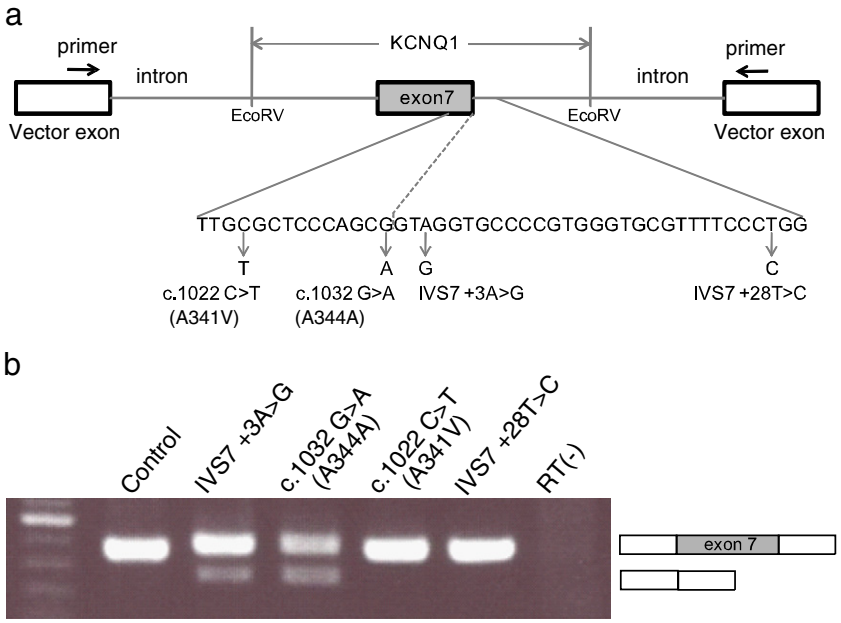

Fig. 3. Minigene analysis. (a) The structure of the minigene harboring KCNQ1 exon 7 (dark shaded box) and its flanking introns (lines between EcoRV sites) inserted into the pSPL3 vector. Open boxes and its flanking lines indicate pSLP3 vector exons and introns, respectively. Arrows upon the open boxes indicate the forward and reverse primers for RT-PCR. The locations of mutations studied in the assay are indicated. (b) RT-PCR from COS7 cells transfected with the minigene constructs. Two major bands were identified; one with KCNQ1 exon joined to vector exons, the other with vector exons only.

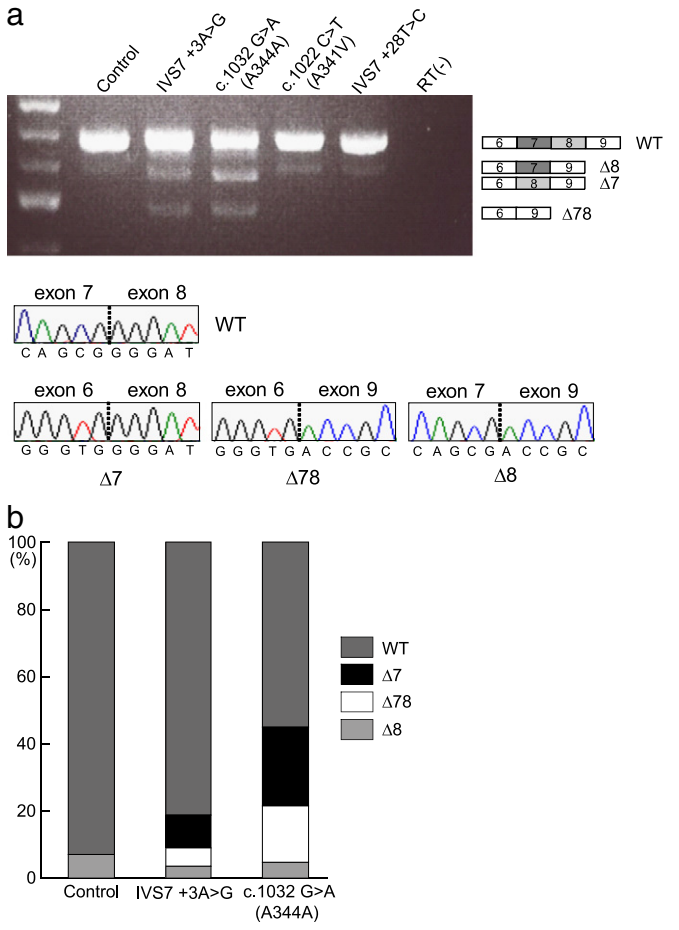

Fig. 4. RT-PCR analysis of patients' blood samples. (a) The result of RT-PCR with total RNA samples extracted from patients' lymphocytes. PCR was performed using primers spanning exons 5 though 10. Nucleotide sequence of each of the exon-skipping mRNAs is also shown. (b) The amounts of WT and mutant mRNAs expressed as a percentage of the total KCNQ1 mRNA. Controls: 4 normal healthy individuals, IVS7 +3A>G: the proband, c.1032G>A: 3 mutation carriers.

Fig. 6b presents regional action potentials of endocardial, mid-myocardial, and epicardial tissues of the 1D model during pacing at 1 Hz in the cases of control (black line), I_{Ks} 60% as a model of IVS7 +3A>G carrier (dark gray line), and I_{Ks} 60% with β-adrenergic stimulation as a model of IVS7 +3A>G carrier under exercise stress (light gray line). Simulated ECGs in the above 3 cases are also shown in the bottom. In the model of IVS7 +3A>G carrier, the β-adrenergic stimulation markedly prolonged the QTc (668 ms) while the I_{Ks} 60% alone did not (388 ms vs. 366 ms in control case).

Similar to Fig. 6b, c presents regional action potentials and simulated ECGs in the cases of control (black line), I_{Ks} 40% as a model of c.1032G>A carrier (dark gray line), and I_{Ks} 40% with β-adrenergic stimulation as a model of c.1032G>A carrier under exercise stress (light gray line). In the model of c.1032G>A carrier, the β-adrenergic stimulation markedly prolonged the QTc (741 ms) while the I_{Ks} 40% alone did not (405 ms).

Fig. 6d and e show regional action potentials and simulated ECGs for a longer period (21–40 s after the first pacing stimulus) in the cases of I_{Ks} 60% (IVS7 +3A>G carrier) with β-adrenergic stimulation and I_{Ks} 40% (c.1032G>A carrier) with β-adrenergic stimulation, respectively. Intriguingly, no arrhythmia was induced for IVS7 +3A>G carrier model (Fig. 6d) whereas tachyarrhythmia was induced for c.1032G>A carrier model (Fig. 6e). In the latter, the monomorphic ventricular tachycardia (VT) was initially derived from triggered activities due to delayed afterdepolarization (asterisks) in the epicardial region. The VT soon degenerated into the fibrillation-like activities (VF) because of marked long APD in the mid-myocardial region, causing decremental conduction (†, endocardial to mid-myocardial regions) followed by propagated graded response (mid-myocardial to endocardial regions) and phase-2 reentry (‡, epicardial activation originating from action potential plateau in the mid-myocardial region).

4. Discussion

4.1. Identification of the novel splicing mutation using minigene assay

A significant fraction of disease-causing mutations affect pre-mRNA splicing. In the present study, three potential splice mutations as well as one definite splice mutation (c.1032G>A) in the intron 7 5′ splice-site

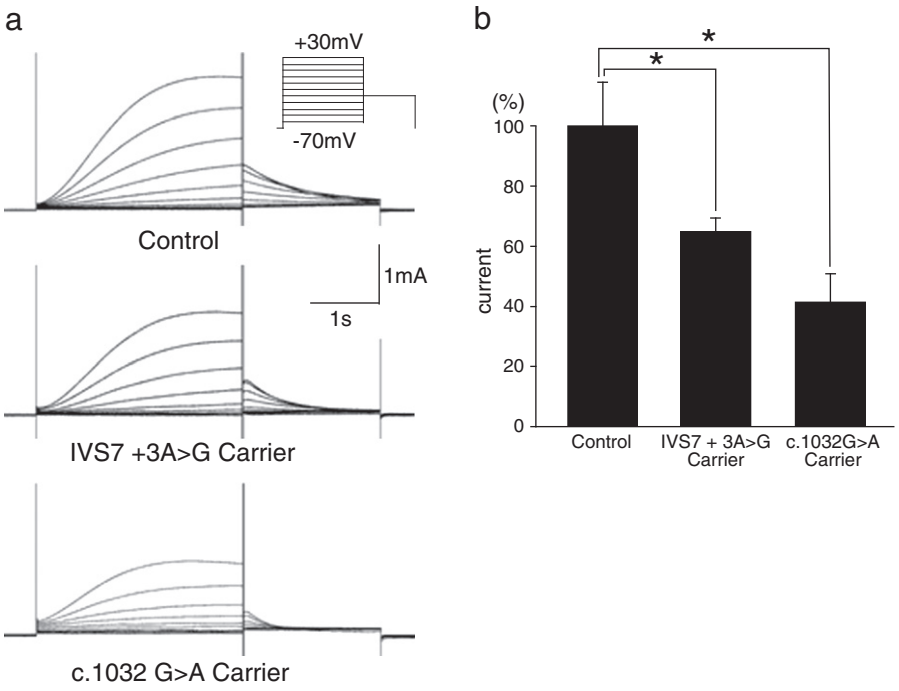

Fig. 5. Electrophysiological analysis. (a) Representative current traces recorded from two-electrode voltage-clamp of *Xenopus* oocytes simulating the proportions of mRNA of control individuals and mutation carriers. Currents were recorded at various membrane potentials from −70 to +30 mV for 3 s in 10 mV increments from a holding potential of −80 mV. A total of 10 ng of cRNA was injected with the relative ratios of WT and mutant KCNQ1 inferred from the data obtained in the real-time RT-PCR experiment. All the current recordings in the present study were performed in the presence of KCNE1 β-subunits (1 ng). (b) Pooled data of currents. Current amplitudes were measured at 1.8 s after the initiation of 3-s pulse applied to a +30 mV test potential. Background I_{Ks} current (22.9 nA) was subtracted. n = 7 for control, 8 for IVS7 +3A>G and 7 for c.1032G>A. *p<0.01 vs. control.

of KCNQ1 identified in clinically-diagnosed LQTS patients were studied. First, we assessed the effects exerted by these mutations on splicing of the KCNQ1 transcript using a hybrid minigene in transient transfection experiments, and found that c.1032G>A and IVS7 +3A>G resulted in the skipping of KCNQ1 exon 7 (Fig. 3). In good agreement with the minigene assay results, we confirmed the presence of exon-skipping transcripts in the blood samples of the mutation carriers (Fig. 4a). The minigene assay is a useful tool to screen for potential splicing mutations in clinically-diagnosed LQTS patients with no mutation in the KCNQ1 coding sequence.

4.2. Mechanistic basis of splicing abnormality

Splice sites are conserved sequences at both ends of an intron that are recognized during the initial steps of splicing [24]. Mutations at 5′ splice-site are frequent among mutations that cause human diseases [25,26]. The human 5′ splice-site consensus sequence is MAG/GT***R***AGT (M is A or C; R is A or G), spanning from position −3 to position +6 relative to the exon–intron junction. A (59%) and G (35%) are conserved at position +3 [27], but it has been shown that 5′ splice-site with disease-causing +3A>G mutations are frequently associated with non-consensus nucleotides at positions +4 and +5 [28]. Indeed, the KCNQ1 intron7 5′ splice-site sequence, GCG/GTA***G***GT, has non-consensus G at position +4, which presumably facilitates the skipping of exon under +3A>G mutation. These dependencies between +3 (A/G) and +4/+5 were demonstrated by other investigators'in in vitro experiment; the splicing defect in the +3A>G mutant was successfully fixed by converting either +4 or +5 independently to the consensus [28]. In contrast, G at position-1 is more strictly conserved, and mutations at this position, as c.1032G>A, cause robust splicing defects [28]. Hence, these differences in the strength of 5′ splice-site sequence dictate the extent to which splicing is disrupted, as indicated by the greater amount of exon-skipped transcripts in c.1032G>A compared with IVS7 +3A>G (Fig. 4b).

4.3. Significance of quantitative assessment of splicing abnormality in risk stratification

The family with IVS7 +3A>G splicing mutation showed mild LQTS phenotype; asymptomatic and had no history of sudden cardiac death, despite an exercise-induced QT prolongation (Fig. 1). Meanwhile, c.1032G>A mutation, a similar KCNQ1 splicing mutation, was more malignant; 8 families out of 9 were symptomatic with episodes of syncope (mostly during exercise or swimming) or sudden death, as we previously reported [10]. These observations strongly suggest the possible correlation between genotypes and clinical phenotypes in LQTS caused by aberrant splicing of KCNQ1. This profound suppression in I_{Ks} currents may underlie the pathophysiology of these patients. Moreover, the level of aberrant proteins may parallel the clinical severity.

We previously showed that the exon-skipping mutant channel subunits (Δ7, Δ7-8, or Δ8) are non-functional, and they have mutant-specific degree of dominant-negative effect on WT channels, by trapping WT intracellularly and thereby interfering its translocation to the plasma membrane [10]. On the assumption that as the result of splicing error the reduction in potassium current would occur in the mutant carriers with similar degrees evaluated by the real-time RT-PCR (Fig. 4b), we estimated functional consequences of these splicing mutation (IVS7 +3A>G and c.1032G>A). Ratios simulating the proportions of various transcripts of KCNQ1 in affected individuals resulted in a pronounced reduction in the whole-cell potassium current in *Xenopus* oocytes, compared with ratios simulating those in normal individuals; 64.8% for IVS7 +3A>G, and 41.4% for c.1032G>A (Fig. 5b).

The computer simulation study (Fig. 6) incorporating these quantitative results demonstrated the pronounced QT prolongation under beta-stimulation in both IVS7 +3A>G and c.1032G>A, and the occurrence of tachyarrhythmias only in c.1032G>A. Our computer model was human ventricular model [15] and the parameters for beta-stimulation were based on physiological data reported

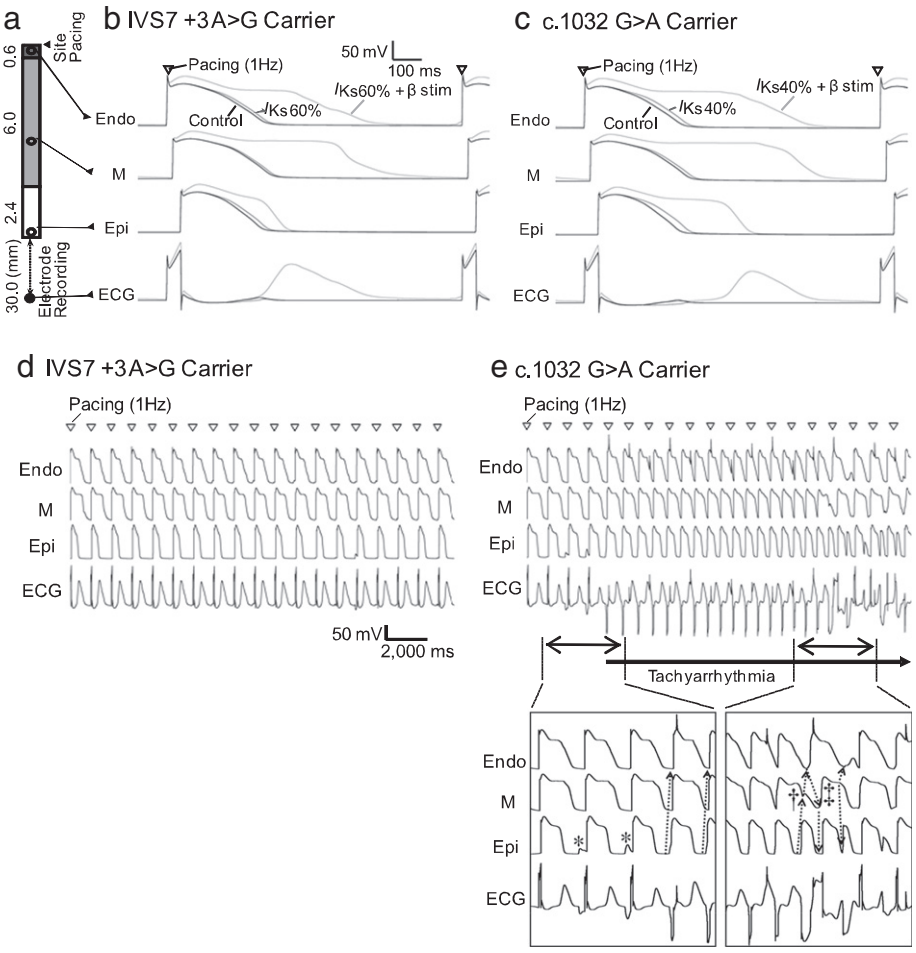

Fig. 6. Computer simulation. (a) One-dimensional myocardial simulated tissue, representing the electrical behaviors of left ventricular free wall. Endo, endocardium; M, mid-myocardium; and Epi, epicardium. Open circles indicate recording sites for regional action potentials, whereas the filled circle represents a unipolar recording electrode for ECG. (b and c) Regional action potentials and simulated ECG during 1 Hz pacing for IVS7 + 3A>G carrier and c.1032G>A carrier, respectively. Open triangles denote timings of 1 Hz pacing. (d and e) No arrhythmia was induced for IVS7 + 3A>G carrier, whereas tachyarrhythmia was induced for c.1032G>A carrier. See text for details.

previously [20–22]. These observations appear to parallel with clinical phenotypes of the mutation carriers; syncopal episodes mainly during exercise in c.1032G>A but not IVS7 + 3A>G patients, whereas asymptomatic IVS7 + 3A>G carriers. Thus, the quantitative assessments of splicing abnormality could be useful in the risk stratification of LQTS patients associated with KCNQ1 splicing mutations.

4.4. Study limitations

Compared to the clinical data on c.1032G>A, those on IVS7 + 3A>G were gathered from two patients, because we failed to conduct the genetic test and clinical tests in their remaining relatives. Because of a relative mildness of their phenotypes, carriers of IVS7 + 3A>G mutation may be less frequently recommended for the genetic test, and this may partially explain why the number of identified IVS7 + 3A>G family was small.

4.5. Conclusions

A novel KCNQ1 splicing mutation IVS7 + 3A>G generates exon-skipping mRNAs, and manifests a mild phenotype of LQTS. The amount of these mRNAs and its functional consequences may determine the clinical severity of the disease.

References

[1] C. Romano, Congenital cardiac arrhythmia, Lancet 17 (1965) 658–659.
[2] O.C. Ward, A new familial cardiac syndrome in children, J. Ir. Med. Assoc. 54 (1964) 103–106.
[3] A.J. Moss, R.S. Kass, Long QT syndrome: from channels to cardiac arrhythmias, J. Clin. Invest. 115 (8) (2005) 2018–2024.
[4] J. Barhanin, F. Lesage, E. Guillemare, M. Fink, M. Lazdunski, G. Romey, K(V)LQT1 and lsK (minK) proteins associate to form the I(Ks) cardiac potassium current, Nature 384 (6604) (1996) 78–80.
[5] M.C. Sanguinetti, M.E. Curran, A. Zou, J. Shen, P.S. Spector, D.L. Atkinson, M.T. Keating, Coassembly of K(V)LQT1 and minK (IsK) proteins to form cardiac I(Ks) potassium channel, Nature 384 (6604) (1996) 80–83.
[6] Q. Wang, M.E. Curran, I. Splawski, T.C. Burn, J.M. Millholland, T.J. VanRaay, J. Shen, K.W. Timothy, G.M. Vincent, T. de Jager, P.J. Schwartz, J.A. Toubin, A.J. Moss, D.L. Atkinson, G.M. Landes, T.D. Connors, M.T. Keating, Positional cloning of a novel potassium channel gene: KVLQT1 mutations cause cardiac arrhythmias, Nat. Genet. 12 (1) (1996) 17–23.
[7] G. Dreyfuss, V.N. Kim, N. Kataoka, Messenger-RNA-binding proteins and the messages they carry, Nat. Rev. Mol. Cell Biol. 3 (3) (2002) 195–205.
[8] A. Kramer, The structure and function of proteins involved in mammalian pre-mRNA splicing, Annu. Rev. Biochem. 65 (1996) 367–409.
[9] N.A. Faustino, T.A. Cooper, Pre-mRNA splicing and human disease, Genes Dev. 17 (4) (2003) 419–437.
[10] K. Tsuji, M. Akao, T.M. Ishii, S. Ohno, T. Makiyama, K. Takenaka, T. Doi, Y. Haruna, H. Yoshida, T. Nakashima, T. Kita, M. Horie, Mechanistic basis for the pathogenesis of long QT syndrome associated with a common splicing mutation in KCNQ1 gene, J. Mol. Cell. Cardiol. 42 (3) (2007) 662–669.
[11] H. Li, Q. Chen, A.J. Moss, J. Robinson, V. Goytia, J.C. Perry, G.M. Vincent, S.G. Priori, M.H. Lehmann, S.W. Denfield, D. Duff, S. Kaine, W. Shimizu, P.J. Schwartz, Q. Wang, J.A. Towbin, New mutations in the KVLQT1 potassium channel that cause long-QT syndrome, Circulation 97 (13) (1998) 1264–1269.
[12] A. Murray, C. Donger, C. Fenske, I. Spillman, P. Richard, Y.B. Dong, N. Neyroud, P. Chevalier, I. Denjoy, N. Carter, P. Syrris, A.R. Afzal, M.A. Patton, P. Guicheney, S. Jeffery, Splicing mutations in KCNQ1: a mutation hot spot at codon 344 that produces in frame transcripts, Circulation 100 (10) (1999) 1077–1084.
[13] L. Crotti, C. Spazzolini, P.J. Schwartz, W. Shimizu, I. Denjoy, E. Schulze-Bahr, E.V. Zaklyazminskaya, H. Swan, M.J. Ackerman, A.J. Moss, A.A. Wilde, M. Horie, P.A. Brink, R. Insolia, G.M. De Ferrari, G. Crimi, The common long-QT syndrome mutation

KCNQ1/A341V causes unusually severe clinical manifestations in patients with different ethnic backgrounds: toward a mutation-specific risk stratification, Circulation 116 (21) (2007) 2366–2375.
[14] T.M. Ishii, C. Silvia, B. Hirschberg, C.T. Bond, J.P. Adelman, J. Maylie, A human intermediate conductance calcium-activated potassium channel, Proc. Natl. Acad. Sci. USA 94 (21) (1997) 11651–11656.
[15] L. Priebe, D.J. Beuckelmann, Simulation study of cellular electric properties in heart failure, Circ. Res. 82 (11) (1998) 1206–1223.
[16] S. Poelzing, F.G. Akar, E. Baron, D.S. Rosenbaum, Heterogeneous connexin43 expression produces electrophysiological heterogeneities across ventricular wall, Am. J. Physiol. Heart Circ. Physiol. 286 (5) (2004) H2001–H2009.
[17] G. Seemann, F.B. Sachse, D.L. Weiss, O. Dossel, Quantitative reconstruction of cardiac electromechanics in human myocardium: regional heterogeneity, J. Cardiovasc. Electrophysiol. 14 (10 Suppl) (2003) S219–S228.
[18] T. Ashihara, T. Namba, T. Yao, T. Ozawa, A. Kawase, T. Ikeda, K. Nakazawa, M. Ito, Vortex cordis as a mechanism of postshock activation: arrhythmia induction study using a bidomain model, J. Cardiovasc. Electrophysiol. 14 (3) (2003) 295–302.
[19] T. Ashihara, N.A. Trayanova, Asymmetry in membrane responses to electric shocks: insights from bidomain simulations, Biophys. J. 87 (4) (2004) 2271–2282.
[20] A. Kobori, N. Sarai, W. Shimizu, Y. Nakamura, Y. Murakami, T. Makiyama, S. Ohno, K. Takenaka, T. Ninomiya, Y. Fujiwara, S. Matsuoka, M. Takano, A. Noma, T. Kita, M. Horie, Additional gene variants reduce effectiveness of beta-blockers in the LQT1 form of long QT syndrome, J. Cardiovasc. Electrophysiol. 15 (2) (2004) 190–199.
[21] C. Terrenoire, C.E. Clancy, J.W. Cormier, K.J. Sampson, R.S. Kass, Autonomic control of cardiac action potentials: role of potassium channel kinetics in response to sympathetic stimulation, Circ. Res. 96 (5) (2005) e25–e34.
[22] J. Zeng, Y. Rudy, Early afterdepolarizations in cardiac myocytes: mechanism and rate dependence, Biophys. J. 68 (3) (1995) 949–964.
[23] T. Ashihara, T. Namba, T. Ikeda, M. Ito, M. Kinoshita, K. Nakazawa, Breakthrough waves during ventricular fibrillation depend on the degree of rotational anisotropy and the boundary conditions: a simulation study, J. Cardiovasc. Electrophysiol. 12 (3) (2001) 312–322.
[24] M.L. Hastings, A.R. Krainer, Pre-mRNA splicing in the new millennium, Curr. Opin. Cell Biol. 13 (3) (2001) 302–309.
[25] M. Krawczak, J. Reiss, D.N. Cooper, The mutational spectrum of single base-pair substitutions in mRNA splice junctions of human genes: causes and consequences, Hum. Genet. 90 (1–2) (1992) 41–54.
[26] K. Nakai, H. Sakamoto, Construction of a novel database containing aberrant splicing mutations of mammalian genes, Gene 141 (2) (1994) 171–177.
[27] N. Sheth, X. Roca, M.L. Hastings, T. Roeder, A.R. Krainer, R. Sachidanandam, Comprehensive splice-site analysis using comparative genomics, Nucleic Acids Res. 34 (14) (2006) 3955–3967.
[28] X. Roca, A.J. Olson, A.R. Rao, E. Enerly, V.N. Kristensen, A.L. Borresen-Dale, B.S. Andresen, A.R. Krainer, R. Sachidanandam, Features of 5′-splice-site efficiency derived from disease-causing mutations and comparative genomics, Genome Res. 18 (1) (2008) 77–87.